2018-01-01

Combustion Joining Of Regolith Tiles For The Construction Of Launch And Landing Pads On The Moon And Mars

Robert Edwin Ferguson
University of Texas at El Paso, referguson@miners.utep.edu

COMBUSTION JOINING OF REGOLITH TILES FOR THE CONSTRUCTION OF LAUNCH AND LANDING PADS ON THE MOON AND MARS

ROBERT EDWIN FERGUSON II

Master's Program in Mechanical Engineering

APPROVED:

Evgeny Shafirovich, Ph.D., Chair

Arturo Bronson, Ph.D.

Guikuan Yue, Ph.D.

Charles H. Ambler, Ph.D.
Dean of the Graduate School

Dedication

To my parents, for all their encouragement;

To Angela, for standing by me these last years;

To Cody, Rebecca, Christopher, and Rachel, you really can do whatever you can dream.

COMBUSTION JOINING OF REGOLITH TILES FOR THE CONSTRUCTION OF LAUNCH AND LANDING PADS ON THE MOON AND MARS

by

ROBERT EDWIN FERGUSON II, BSME

THESIS

Presented to the Faculty of the Graduate School of

The University of Texas at El Paso

in Partial Fulfillment

of the Requirements

for the Degree of

MASTER OF SCIENCE

Department of Mechanical Engineering

THE UNIVERSITY OF TEXAS AT EL PASO

May 2018

Acknowledgements

I would first like to thank Dr. Evgeny Shafirovich, for his guidance, direction, inspiration, mentoring, and just giving me a chance.

I would like to thank my committee members, Dr. Arturo Bronson and Dr. Guikuan Yue, for their time and attention.

Thank you to all those I've worked with at UTEP, including Gabriel Llauses, Edgar Maguregui, Reina Trevino, Rodrigo Mesta, Travis Belcher, Justin van Hoose, and most especially Sergio Cordova and Alan Esparza for all their help and guidance.

Thank you to Dr. James G. Mantovani of the Granular Mechanics and Regolith Operations Lab at Kennedy Space Center for the support and direction.

This material is based up on work supported by the National Aeronautics and Space Administration under Grant Number NNX16AT16H issued through the NASA Education Minority University Research Education Project (MUREP) through the Harriet G. Jenkins Graduate Fellowship activity.

Abstract

Combustion-based methods are attractive for space manufacturing because the use of chemical energy stored in reactants dramatically decreases the required external energy input. Recently, a sintering technique has been developed for converting lunar/Martian regolith into ceramic tiles, but it is unclear how to build a reliable launch/landing pad from these tiles with small amounts of energy and materials. Here the feasibility of joining regolith tiles using self-propagating high-temperature reactions between two metals powders is explored. Combustion of a 1:1 molar aluminum/nickel mixture placed in a gap between two tiles, made of JSC-1A lunar regolith simulant, was studied in an argon environment at 1 kPa pressure. Stable propagation of the combustion front was observed over the tested range of distances between the tiles, 2 – 8 mm. The front velocity was found to increase with increased spacing between the tiles. Joining of the tiles was achieved in several experiments and improvement with increasing the tile thickness was observed. Measurements of the thermophysical properties of the tiles, the reactive mixture, and the reaction product revealed that thermal diffusivity of the product is higher by two orders of magnitude than that of the initial mixture or the tiles. A model for steady propagation of the combustion wave over a condensed substance layer placed between two inert media was applied for analysis of the investigated system. Testing the model with different values from the obtained range of thermal diffusivities has resulted in reasonable agreement between the experimental and modeling dependencies. Both the experimental and modeling results indicate that the quenching distance in the investigated system is lower than 2 mm, which implies that a small amount of the reactive mixture would be required for sintering regolith tiles on the Moon.

Table of Contents

List of Tables

List of Figures

Chapter 1: Introduction

Recently, interest in manned landings on the Moon and Mars has increased, not only in the United States, but in countries with emerging space programs such as China, India, and South Korea, as well as private enterprises such as Space X and Blue Origin. This increased attention has revived a problem from the Apollo landings that has not yet been satisfactorily resolved- the problem of dust mitigation. The lunar surface is covered in a layer of loose rock and dust known as regolith. This layer is thought to be up to 15 m thick in the highland areas of the region of the Moon, and as little as a few centimeters near some craters. [1] The regolith is thought to be produced by meteorite impact with the bedrock over the lifetime of the Moon; each successive impact breaks up rock as well as turning over fine dust particles. As the layer has deepened over millions of years, however, increasingly violent impacts are required to reach the bedrock in mature locations, and repeated smaller impacts have the effect of turning over the existing dust and smaller rocks. [1]

Dust Mitigation in Lunar/Martian Missions

The top layer of the regolith consists of a very fine dust, gray in color, about 1-2 mm thick. [1,2] It is this loose layer which can pose the greatest danger landing or launching spacecraft, as well as any equipment nearby. Specifically, the exhaust plume from the rocket nozzle can cause failure of the regolith and propel it away from the point of launch/landing. Two such examples of this hazard include the Apollo 12 and 15 landings. During the Apollo 12 descent phase, the astronauts reported the first appearance of a dust plume at approximately 100 ft above the lunar surface. At about 40 feet, the lunar surface was completely obscured. [3] Beyond the danger inherent in landing essentially blind, the Apollo 12 landing was unique in that the landing site was chosen for its proximity to the Lunar Surveyor III unmanned lander. Parts of the craft were removed and returned to Earth. In addition to an overall wear of these sections from exposure to the lunar environment, sections facing Apollo 12 were found to be pitted with dust and debris from

the landing less than 200 m away. [4,5] Based on analysis of the parts, it is estimated that the particles reached velocities of up to 2000 m/s, approaching the escape velocity of the Moon. [4] In the case of Apollo 15, visibility was lost approximately 60 feet above the surface, and at 30 feet began to affect the landing radar. [3] As a result, the astronauts were unable to identify the rim of a crater at the landing site. Upon landing, the lunar module rocked 11° from vertical and came to rest on three legs, with the fourth lifted off the surface and supporting no weight. [5] Clearly, based on these examples, blowing dust is a significant hazard during lunar operations, and is expected to be on Mars as well. Moreover, due to the estimated range of such blowing dust, particularly in low gravity, merely landing farther away from established equipment would not only prove to be impractical over time, but ultimately ineffective as a solution as well.

To address these concerns, various techniques of dust mitigation have been investigated. These have included polymer surface stabilization [6], in which a polymer is sprayed on the surface and cured, resulting in a condensed, dust-free surface. In addition, several research groups have investigated ways of consolidating regolith into construction materials, from which launch/landing pads could be constructed. These techniques have included high-temperature sintering [6] as well as combustion synthesis reactions [7-13]. These proposals have the additional benefit of using the regolith found on the Moon or Mars as a base material, a concept known as *in-situ resource utilization* (ISRU). By fabricating materials using ISRU, the amount of material required to be brought from Earth is reduced, thereby reducing the size, complexity, and cost of the overall mission.

Of these, high-temperature sintering of regolith into tiles has been experimentally completed at the Granular Mechanics and Regolith Operations Lab at NASA's Kennedy Space Center [6]. The process involves placing an amount of lunar regolith simulant, JSC-1A, into a ceramic mold and heating to 1125°C. Note that JSC-1A is considered a chemical simulant, with a chemical composition similar to lunar samples, as shown in Table 1.1 [14]. Once cooled, the regolith simulant forms a solid, brick-like tile, in the shape and thickness of the mold. For the application on the Moon or Mars, a solar collector has been considered as a means of sintering

regolith [6]. These tiles have been shown to withstand simulated thruster fire using high pressure nitrogen; however, small gaps between the tiles proved vulnerable to the high velocity gases and became a point of failure for the larger structure [6].

Table 1.1: Chemical Comparison of Lunar Regolith Sample and JSC-1A Simulant.

Constituent	**Apollo 17 Sample 70051**	**JSC-1A**
	Wt.%	Wt.%
SiO2	42.2	45.7
Al2O3	15.7	16.2
CaO	11.5	10.0
MgO	10.3	8.7
FeO	12.4	-
Fe2O3	-	12.4
Na2O	0.2	3.2
K2O	0.1	0.8
TiO2	5.1	1.9
P2O5	-	0.7
MnO	0.2	0.2

SHS and Combustion Joining

To fabricate a structure such as launch/landing pads from these tiles, however, a method of joining them together is desired. Combustion joining, a technique based on the principles of self-propagating high-temperature synthesis (SHS), shows promise as a method for combining the tiles together. SHS involves an exothermic reaction between two condensed materials, usually powders,

in which enough heat energy is produced to heat adjacent material to the ignition temperature, thus producing a self-propagating reaction. [15] Such a reaction will continue until the conditions for combustion are removed, such as exhaustion of the combustible mixture or an increase of heat transfer to the environment to such an extent that the adjacent material cannot reach the ignition temperature. As the combustion front moves forward, the desired reaction product cools in its wake. The technique has the advantage of producing materials with low amounts of impurities, as most volatiles are lost as gas due to the heat of the reaction. However, this tends to result in porous, low density product materials. Of particular interest in the current context is that SHS usually involves a reaction of condensed phase reactants, requiring no oxygen or other gases to occur. [16] In addition, once the reaction has been initiated, no further heat source is required. While this cannot necessarily be considered an energy-saving process, as the pure reactants require additional energy prior to the reaction, it does allow for a limited external energy requirement if the reactants are available. [17]

Combustion joining is the method of applying the techniques of SHS to join two parts together. The reactive mixture is placed into a gap between two parts and ignited, simultaneously producing heat to melt the edges of the parts and forming a molten product to join the two pieces together. Perhaps the most widely known example is the use of “thermite” reactions involving aluminum and a metal oxide. [18] Such a reaction, involving iron oxide, is used to weld railroad tracks together. The aluminum reduces the iron oxide, producing a two-phase product of alumina and pure iron. Together with the heat of the reaction, this technique would join the tracks together via the product (iron). Note that gravity may separate such multiple products based on density.

The present work intends to apply the techniques of combustion joining to the problem of joining regolith tiles together. JSC-1A regolith simulant begins to melt at 1120°C [14], a temperature readily achievable by SHS reactions. For the purposes of these experiments, a nickel-aluminum intermetallic mixture was chosen. Thermodynamic calculations done using THERMO software suggest an adiabatic combustion temperature of 1912 K (1639°C) for this mixture, with the product 42% liquid/ 58% solid immediately following combustion. This is well above the

expected melting point of the tiles, which should therefore interact with the molten combustion product. Intermetallic reactions also have the added benefit of a single phase product, while many thermite reactions often result in a two-phase product which may separate due to gravity. It is believed that such a two-phase product would reduce the properties of the joining.

Research Objectives

The goals of this research are to investigate the feasibility of using combustion joining to combine sintered regolith tiles into larger structures. As described above, a nickel-aluminum mixture was chosen to ensure a single product compound. To better understand the combustion propagation, the thermophysical properties of the relevant materials, including the JSC-1A regolith tiles, the Al/Ni reactive mixture, and the NiAl product were to be determined. These included the density, thermal diffusivity, and specific heat of each material, from which the thermal conductivity of each could be calculated. With this information, an appropriate model was to be examined for the combustion front propagation, to allow the process to be scaled up at some point in the future, if desired.

Chapter 2: Experimental

Testing of the combustion joining involved several pieces of equipment at various stages. The process can be generally divided into tile preparation, powder preparation, and combustion testing, as well as separate testing of the thermophysical properties of the regolith tiles.

Tile Preparation

The tiles were prepared from JSC-1A lunar regolith simulant. The simulant is stored in an enclosed bin at the Granular Mechanics and Regolith Operations Lab on Kennedy Space Center, Florida. The bin is located indoors, but should not be considered to be airtight. The JSC-1A simulant was removed as necessary and placed into pre-made ceramic molds. These molds, with simulant, were then placed into an oven at 200°C for several hours to remove residual moisture from both the regolith and the ceramic. The molds were then removed to a ceramics kiln located outside of the lab for firing. The simulant was heated to 1125°C over the course of 4-6 hours, and held at that temperature for one hour. Following the temperature hold, the tiles were allowed to cool naturally to ambient temperature overnight, resulting in a tile as shown in Figure 2.1. The final tiles were approximately 100 mm square with rounded corners, and three different thicknesses of 9.2 ± 0.5, 17.2 ± 0.4, and 27.5 ± 0.6 mm. The tiles were then removed from the molds and secured in Ziploc bags for transportation to the University of Texas at El Paso.

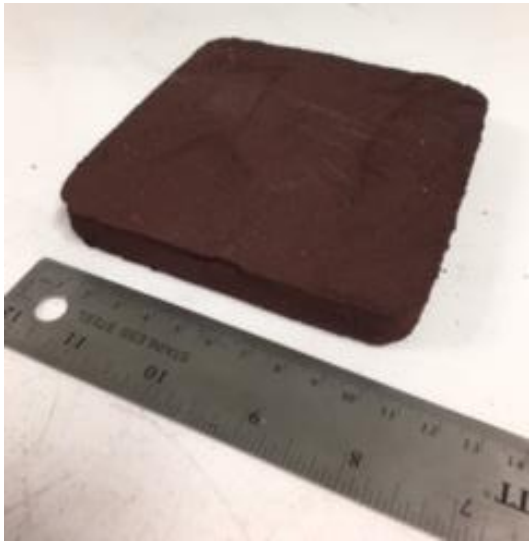

Figure 2.1: Regolith tile, as received from KSC.

Once received at UTEP, the tiles were cut into the required sizes for combustion experiments. Experiments were conducted using either 32 mm square or 32 mm x 64 mm rectangular shapes, keeping the original thickness of the tiles. The tiles were arranged on a brass tile holder in arrangements of 4 square or 2 rectangular tiles. An experimental powder gap of 2, 4, 6, or 8 mm was established between the tiles using steel pins of respective size. The tiles were held in place horizontally and vertically by two sets of two brass retaining bars secured by threaded bolts. In some experiments, a 27.5 mm tile was cut so as to create an equivalent stack of two tiles, and a C type thermocouple (95%W/5%Re-74%W/26%Re, wire diameter 76.2 µm, Omega Engineering) centered between them before the powder was added. In such cases, the overall height of the tiles was reduced to 25.4 ± 0.6 mm. Thermal paper (3-6 mm thickness) was used to protect the tile holder surface from the reaction heat, as well as reduce heat losses to the base of the tile holder. Once the tiles were properly loaded into the holder, the entire apparatus was moved into the glove box for powder loading.

Powder Preparation

The nickel and aluminum powders were purchased from Alfa-Aesar. The aluminum powder was 97.5% pure, with a particle size of 3.0-4.5 μm. The nickel powder was 99.9% pure, with a particle size of 3-7 μm. Both powders were used as delivered from the vendor; no additional milling was done. The powders were measured to a 1:1 molar ratio under a nitrogen environment in the glovebox. The powders were combined into a mixing container and sealed. The sealed container was then removed from the glovebox and secured in a three dimensional inversion kinematics mixer (Inversina 2L, Bioengineering) for one hour for mixing of the powders (see Figure 2.2). The container was then returned to the nitrogen environment of the glovebox and opened. The mixed powder was placed into a plastic storing container and the container secured inside a desiccator in the glovebox.

Figure 2.2: Inversina 2L 3-D Inversion Kinematics Mixer.

Once the tile holder was loaded and placed into the glovebox, the powder container was removed from the desiccator. The tile holder was secured onto a Gilson SS-28 Vibra-Pad shaker.

The mixed Ni-Al powder was placed into the gap(s) between the tiles using a lab spatula until the void was filled. The shaker was turned on, allowing the powder to settle into the gap. Additional powder was added until the powder level settled at the top of the tiles. The shaker was then left on for an additional five minutes to ensure settling. This procedure was used to ensure a uniform density throughout the powder mixture.

Combustion Experimental Setup

The tile holder, now loaded with both tiles and powder, was placed into a plastic container and removed from the glovebox. The container was moved to the laser ignition facility, an 11.35 L stainless steel chamber, as shown in Figure 2.3. The chamber is equipped with two window and two door ports, as well as a zinc selenide window at the top to accommodate laser ignition. The chamber is also equipped with a pressure transducer and thermocouple leads, as well as a connection for a compressed gas cylinder. A relief valve and rupture disc are installed to prevent over-pressurization of the chamber. The relief valve is set for 10 psig, while the rupture disc is designed to burst at 28±2 psig. A GoPro Hero Session camera with a wireless internet connection was installed inside the chamber, looking down, to record the combustion experiments. The GoPro camera can be operated from any smartphone. Video was recorded on an SD card at 60 frames/s.

Figure 2.3: Laser Ignition Vacuum Chamber.

The laser directed into the combustion chamber is a Firestar ti-60, an air-cooled 60W CO_2 laser. A beam bender re-directs the beam into the top of the chamber through the ZnSe window. The laser is aligned using a red visible laser diode pointer installed in the system. The infrared beam of the actual laser is invisible to the naked eye. The laser emits a wavelength of 10.55-10.68 μm, with a beam on 2.0±0.3 mm. The laser is controlled via a LabView program on the adjacent PC. A photo resistor is used to switch off the laser beam after ignition occurs. In addition, the laser is equipped with a kill switch and flashing warning light during operation. A Synrad UC-2000 controller is used to set the laser at the appropriate power setting (95% of maximum, in this work).

Once the loaded tile holder was placed inside the chamber, the beam was aligned using the laser diode pointer. The beam was aimed at the center of the tiles in a 4-tile experiment, and close to one end in a 2-tile experiment. This was done to maximize the distance (about 50 mm) traveled by the combustion front in 2-tile experiments to facilitate velocity measurements. When the beam was properly aligned, the chamber was sealed. All windows were covered with aluminum foil to minimize laser exposure except one to allow for lighting via a pair of LEDs. A vacuum pump

(Fischer Scientific Maxima C Plus) was started, reducing the chamber to below 1 kPa. The vacuum valve was closed, and a second valve opened to allow the chamber to be re-pressurized with argon gas. Once atmospheric pressure was achieved, the valve was closed. In this way, the system was purged of air a total of three times. After the third time, the pressure in the chamber was reduced to an argon atmosphere of 1 kPa. At this time, all valves were closed and the chamber was considered sealed. The camera, pressure transducer, and any thermocouples were set to record. The laser was engaged, igniting the powders and initiating a combustion front which traveled the length of the powder, as shown in Figure 2.2. Once the combustion front was complete, the laser was placed in safe mode and the argon flow was restarted to return the chamber to atmospheric pressure. After pressure reached equilibrium, an outgassing valve was opened, relieving the excess argon to the lab exhaust system. The chamber was purged in this manner for five minutes, at which time the argon flow was closed and the chamber was opened.

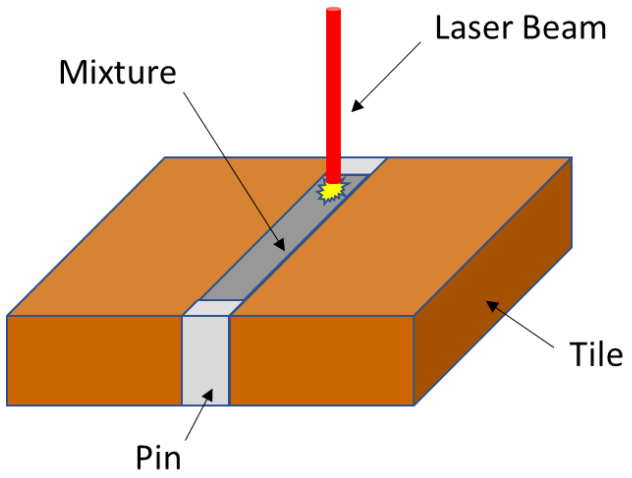

Figure 2.4: Schematic of the Experimental Configuration.

Early combustion testing focused on establishing the procedure and experimental setup, as well as verifying that the combustion front would propagate between the tiles. Later testing focused

on determining the combustion front velocity and temperature. Video analysis for the front velocity was done using Wondershare Filmore v8.5.0 video editing software.

Determination of Thermophysical Properties

To better understand and model the reaction propagation between the tiles, it is necessary to know the thermophysical properties of the materials involved. While some information is-available in literature, specific information about the powder mixture and the regolith tiles was unavailable.

The specific heats of the materials were tested using a Netzsch DSC 404 F1 Pegasus differential scanning calorimeter, shown in Figure 2.5. Testing was conducted under a 70 mL/min argon flow using platinum crucibles with lids. Because platinum may affect melting or reaction temperatures, an alumina liner was placed inside the crucible for testing involving the NiAl product. First, a correction file was established using the crucible with no sample. Consecutive tests were then conducted using a sapphire standard provided by Netzsch and the material to be tested. In each case, the same crucible was used and the temperature profile consisted of a heating phase to 40°C, where the temperature was held for 5 min, followed by the testing phase where the temperature was increased at 10°C/min. The specific heat was determined by the Netzsch Proteus Version 6.1.0 using the ratio method, shown in Equation 1, based on the known specific heat profile of the sapphire standard. Testing was conducted in accordance with Netzsch recommendations in the range of 40-500°C for regolith tiles and the NiAl product. For the Ni-Al powder, testing was conducted from 40-125°C to avoid any reactions.

$$c_{p,sample} = \frac{m_{standard}}{m_{sample}} * \frac{DSC_{sample} - DSC_{baseline}}{DSC_{standard} - DSC_{baseline}} * c_{p,baseline} \quad (1)$$

In addition to determining specific heats of experimental materials, the DSC was also used to verify the melting point of the regolith tiles. While this information was available in literature for JSC-1A lunar simulant, it was not specifically reported for the sintered tiles. A DSC test was

therefore run using a 47.1 mg tile sample in an alumina crucible heated at a rate of 10 °C/min to a maximum temperature of 1250°C to confirm the melting point (argon flow rate 70 mL/min).

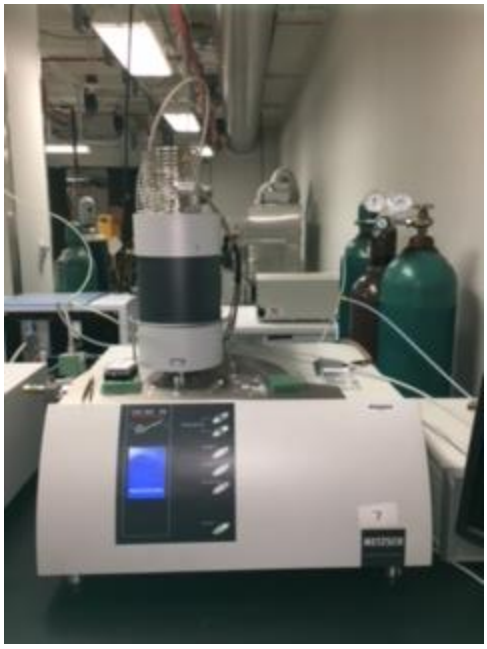

Figure 2.5: Netzsch DSC 404 F1 Pegasus Differential Scanning Calorimeter

Thermal diffusivities were determined using a Netzsch LFA 457 MicroFlash laser flash analysis instrument, as shown in Figure 2.6. A disc-shaped sample of the tested material, approximately 12.5 mm in diameter, was coated in graphite and placed into an aluminum titanate sample holder inset with a silicon carbide cap. To test the Al/Ni powder mixture, a sapphire pan and lid was used. Testing was conducted at temperatures up to 500°C in argon environments with a flow rate of 20 mL/min. Again, Al/Ni reactive mixtures were only tested to 125°C to prevent reactions in the equipment. In each case, the instrument stabilized the temperature at preprogrammed steps and completed a series of laser “shots” to determine the thermal diffusivity of the tested material.

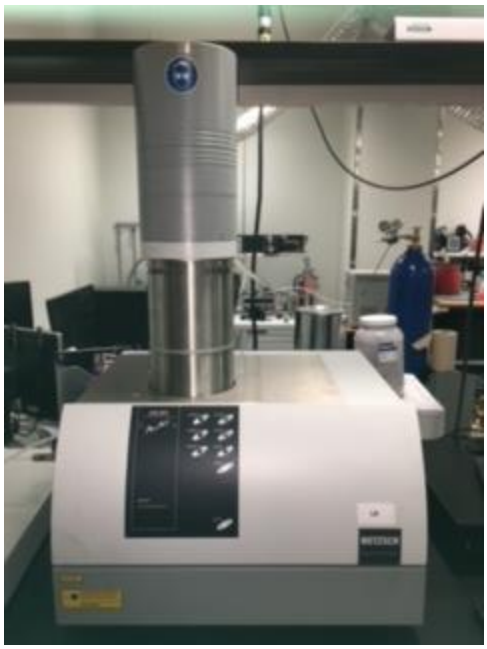

Figure 2.6: Netzsch LFA 457 MicroFlash Laser Flash Analysis Instrument.

Finally, an X-ray diffraction test was conducted of the combustion products to confirm their composition. The test was conducted using a Bruker D8 Discover XRD, Cu K-alpha 1, 0.154 nm. The scan was conducted in a 2θ range of 10 to 90° with a scan speed of 1 °/min and a step size of 0.02°

Chapter 3: Experimental Results

Thermophysical Properties

The melting point of the JSC-1A tile was verified by a DSC measurement. Figure 3.6 presents the obtained DSC curve, which shows the same events that were observed in the previously reported DTA curve for the original, not sintered, JSC-1A simulant [14]. The first endothermic peak and the subsequent exothermic peak correspond to the glass transition and the glass crystallization events, respectively, while the large endothermic peak beginning after 1100°C indicates melting. That the tiles melt at temperatures well below the calculated adiabatic flame temperatures of the Al/Ni combustion (1639°C) supports the hypothesis about the potential positive effect of melting on the combustion joining.

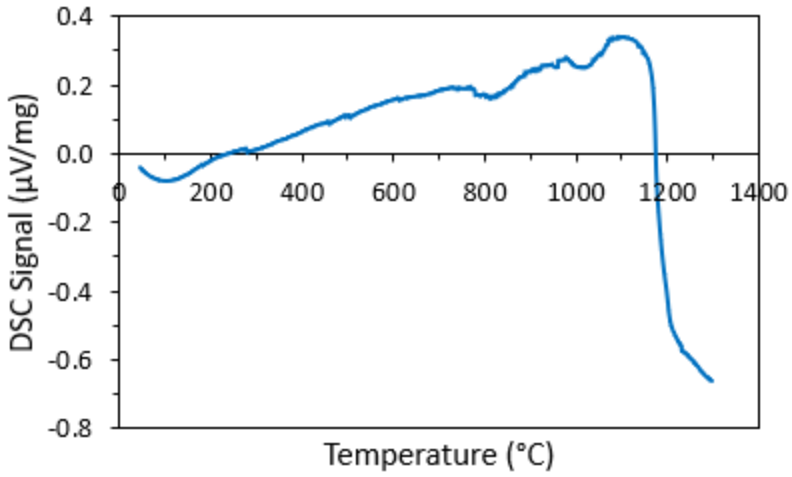

Figure 3.6: DSC Curve of JSC-1A Lunar Regolith Simulant Tiles.

In the DSC measurements of specific heats, the results obtained for the tiles, the Al/Ni reactive mixture, and the NiAl product are shown in Figure 3.7. As previously stated, the Al/Ni mixtures measurements were kept below 125°C to ensure no reaction occurred.

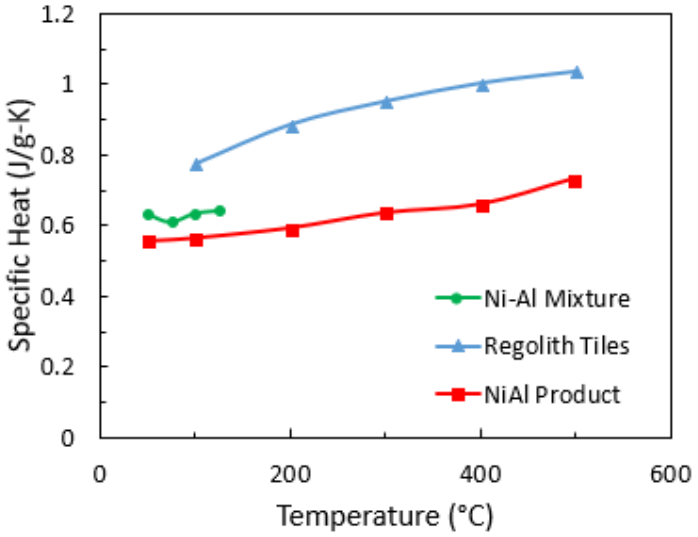

Figure 3.7: Specific Heats of Regolith Tiles, Ni-Al mixture, and NiAl Product.

The laser flash analysis revealed the NiAl product to have a much higher thermal diffusivity than the other two materials. For this reason, the results are shown in two figures (Figures 3.8 and 3.9). Note that the error bars correspond to one standard deviation.

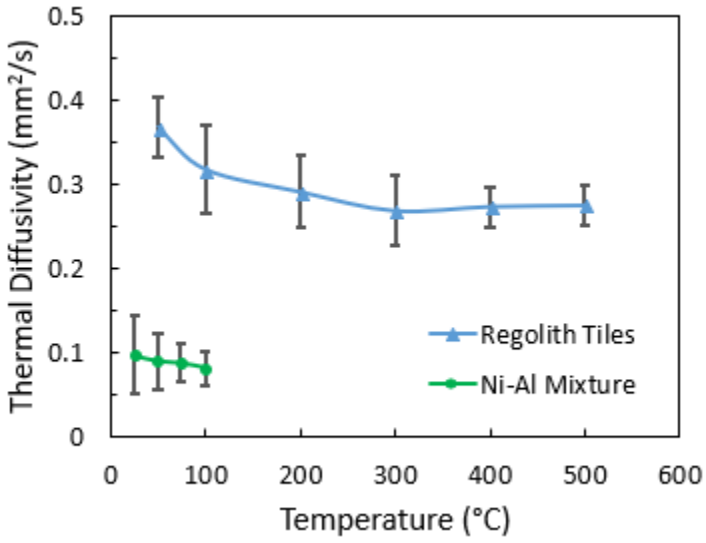

Figure 3.8. Thermal Diffusivity of the Reactive Mixture and the JSC-1A Tiles.

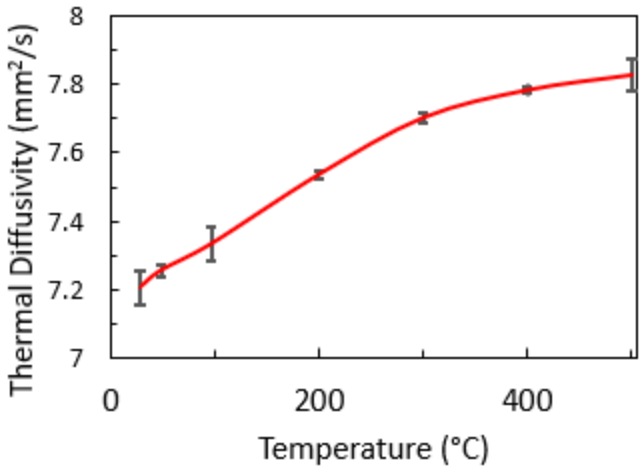

Figure 3.9. Thermal Diffusivity of the NiAl Product.

The determination of the thermophysical properties was performed with the goal of providing data for the combustion model that neglects their temperature variations and it was decided to use the specific heats and thermal diffusivities at 500°C. Since the experimental data for the Al/Ni mixture was only obtained up to 125°C, a comparison with the literature data on specific heats of Al and Ni was conducted. At a temperature of 400 K (127 °C), specific heats of Al and Ni were equal to 25.78 and 28.46 J/mol-K, respectively [19]. This leads to the specific heat of Al/Ni equimolar ratio being equal to 0.633 J/mol-K, which is close to the obtained measurements. Since the specific heats of Al and Ni are changing with increasing temperature, for consistency the specific heat used for the Al/Ni mixture (1:1 at%) was 0.719 J/g-K, based on literature data at 800 K (523°C) [19]. Note that this value coincides with the specific heat of the NiAl product at 500°C. Regarding thermal diffusivity, it was decided to use the value 0.10 mm^2/s, close to the experimental data at 23-100°C.

The densities of all tested materials were calculated based on the measurements of mass and volume at room temperature (23°C). The density of the Al/Ni mixture was determined in its location in the sample holder after the vibrating procedure. The obtained value corresponds to approximately 40% relative density (the theoretical density of a non-porous Ni-Al mixture is 5.164

g/cm^3). The thermal conductivity of each material was then calculated based on the thermal diffusivity, specific heat, and density. Table 1 shows the values of the thermophysical properties that were accepted for use in modeling.

Table 3.1: Thermophysical Properties of the Studied Materials.

Material	**Thermal diffusivity**	**Specific heat**	**Density**	**Thermal conductivity**
	mm^2/s	J/g-K	g/cm^3	W/m-K
Tiles	0.268	1.038	1.84±0.20	0.512
Reactive mixture	0.1	0.719	2.10	0.151
Product	7.83	0.72	2.21±0.16	12.46

The XRD analysis (Figure 3.10) confirmed that the combustion product NiAl. All observed peaks correspond to a single NiAl phase.

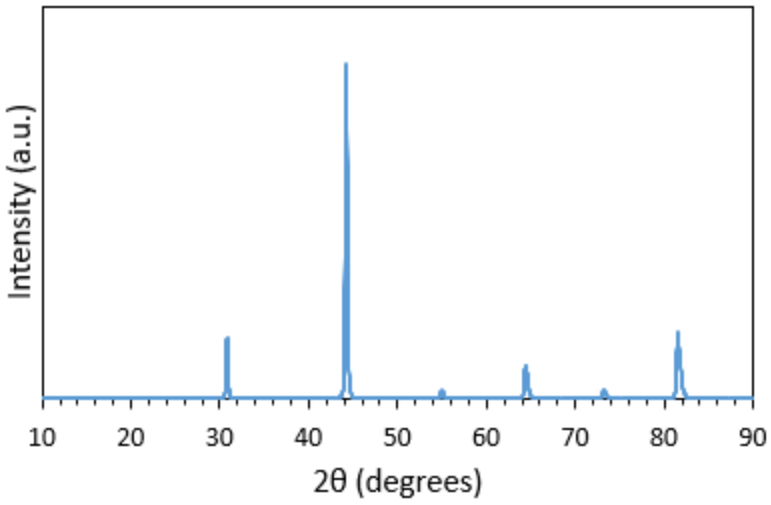

Figure 3.10: XRD Results of Combustion Product.

Combustion Characteristics and Products

Initial testing involved two or four tile arrangements of varying sizes. The laser was aimed at the center of the tile holder, and combustion front propagation moved outward. Combustion front propagation was found to occur regardless of experimental gap size (2, 4, or 6 mm). Joining, however, was inconsistent. Testing with smaller gap size (2 mm) and thinner tiles (9.2 mm) failed to join during any testing. Larger gaps (4 mm and wider) and thicker tiles (17.2 and larger) were found to join together, albeit not on a consistent basis. This was expected, as the larger gap sizes obviously hold more powder, and lead to a higher combustion temperature, while thicker tiles have a larger surface area exposed to the high temperatures and reaction products. These initial tests showed that it was possible to join the tiles using the Ni-Al system, at least to the extent that the tiles could support their own weight (see Figures 3.11 and 3.12).

Figure 3.11: Joining of two 12.7mm tiles.

Figure 3.12: Joining of four 12.7mm tiles.

In addition, temperature readings were taken during some of these early tests. An example of one such test is shown below in Figure 3.13. Note that the electromotive force is shown, not the temperature reading. This is due to the use of C type thermocouples (tungsten-5% rhenium and tungsten-26% rhenium), for which the relation between temperature and emf is non-linear. For clarity, the temperature associated with certain emf readings is included. The particular experiment shown involved 17.2 mm thick tiles with a 4mm experimental gap. In this test, a temperature of 1410°C was achieved, followed by a rapid cooldown of 900°C in the immediate 40 s.

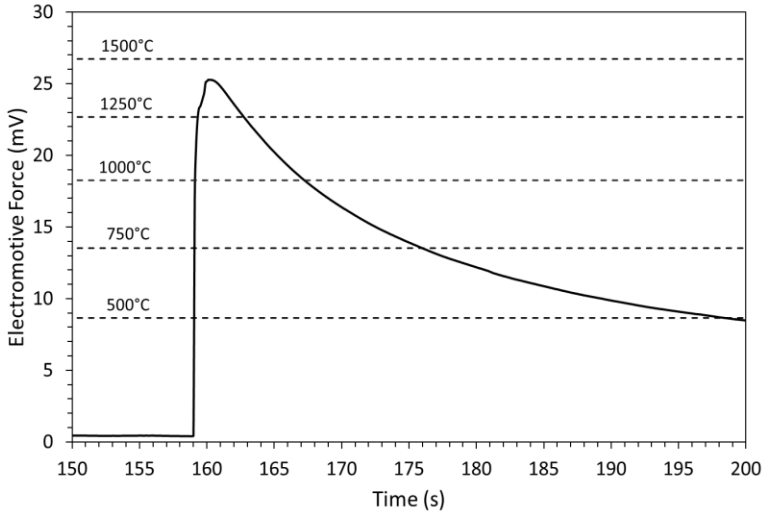

Figure 3.13: Temperature Profile of JSC-1A Tiles with 4mm Gap.

Additional testing focused on determining the combustion front velocity and temperature. A total of 20 experiments were conducted, with five experiments conducted at each experimental gap. The gaps tested were 2, 4, 6, and 8 mm, all using 27.5 mm tiles. In four of these experiments, one at each gap size, the tile was cut in half horizontally. Each of the two original tiles was thereby replaced with a stack of two tiles of roughly the same size, with a thermocouple wire held in place by the two tiles. The thermocouple was placed so as to align the junction as closely as possible with the center of the combustion front. The thermocouple readings for 2-mm and 4-mm experimental gaps are shown in Figure 3.14. Because of the highly non-linear temperature relation of Type C thermocouples, the electromotive force is shown on the y-axis, with dashed lines indicating index temperatures. It is apparent that the 4-mm gap experiment produced higher temperatures than a 2-mm gap. This is to be expected, as the 2-mm gap will be subjected to higher heat losses relative to the size of the combustion front. Similar results were seen with a 6-mm gap. When an 8-mm gap was tested, however, the corresponding temperature was found to be significantly higher than the adiabatic flame temperature. This is likely due to an interaction between the molten nickel-aluminum product and the tungsten-rhenium alloys of the C-type thermocouple wire (tungsten-aluminum intermetallics have been previously reported in literature [20]). As a result, the relationship between gap size and combustion temperature could not be reliably determined.

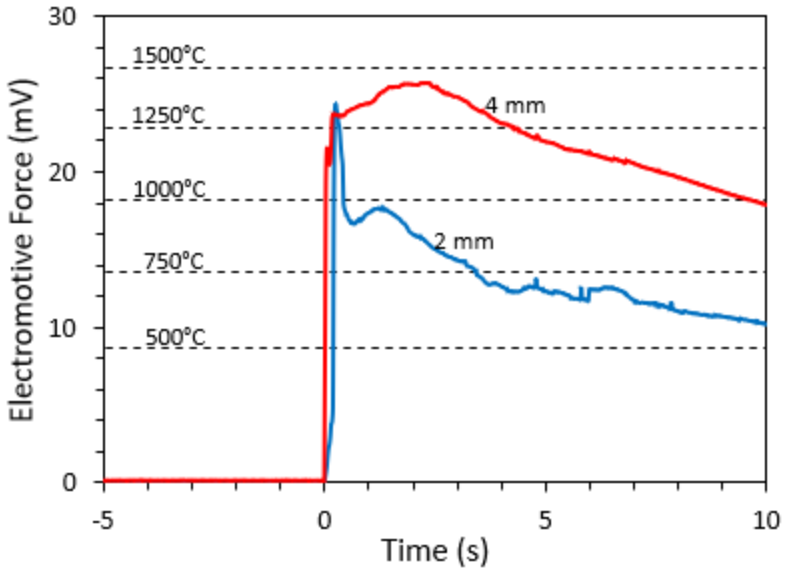

Figure 3.14: Thermocouple Readings During Combustion at 2-mm and 4-mm Gaps.

The combustion front velocity was found to increase with increasing gap size, as shown in Figure 3.15. The velocity curve appears to be leveling off, with smaller velocity increases with each increase in gap size. This is expected, as the combustion front eventually should reach a maximum combustion velocity for a given mixture and circumstances.

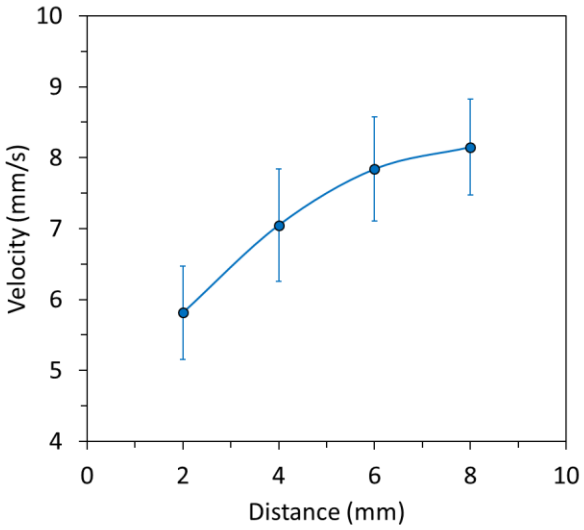

Figure 3.15: Combustion Front Velocity with Respect to Experimental Gap Size.

Despite the increasing gap sizes and larger amount of reactive mixture, however, joining remained poor. During some tests, the joining was strong enough to support the tile weight as before. In many tests, the NiAl product joined to one but not both of the tiles, or not at all. Because the densities of the reactants and products are nearly the same, this does not appear to be the result of shrinking of the product. It is likely a result of the combustion temperature not raising the temperature of the tiles sufficiently high to melt. Note that the above temperatures were recorded at the center of the combustion front, not at the edge near the tile. It is also possible that the thermal contraction of the product material and/or tiles during cooling pulled the NiAl product off one or both of the tiles, as the tiles were unable to move with such a contraction due to the braces and pins.

Chapter 4: Combustion Modeling and Discussion

To better understand the combustion process during these experiments, it was desired to produce a mathematical model. This would also allow the process to be scaled up at some future time, if desired.

Model Formulation

A two-dimensional model for steady propagation of the combustion wave over a condensed substance layer placed between two inert media has been analyzed in [21,22]. Since the distance between the tiles in our experiments was 2-8 mm and their height was 27.5 mm, the two-dimensional model can be applied, with caution, to the investigated system (the effect of the finite height increases with increasing distance between the tiles). Different types of this sandwich-shape configuration were considered in [21,22]: (1) thermally *thick* combustible layer and thermally *thick* inert media, (2) thermally *thick* combustible layer and thermally *thin* inert media, (3) thermally *thin* combustible layer and thermally *thin* inert media, and (4) thermally *thin* combustible layer and thermally *thick* inert media. It has been shown that, depending on the configuration, the combustible behavior may be different. For example, when both the layer and the media are thermally thin, there are no critical conditions for the flame propagation.

For the combustion joining of regolith tiles on the Moon or Mars, it is desired, of course, to minimize the amount of the combustible mixture. Therefore, it makes sense to consider the case in which the combustible layer is thermally thin. Note that "thermally thin" means that the temperature distribution across the layer is negligible.

In the analysis for combustion of this configuration [21], it has been assumed that heat propagates from the reaction zone to the fresh mixture, and, perpendicularly, to the inert media. Assuming that the heat removed by the inert material is much smaller than the heat that propagates into the fresh mixture, the characteristic thickness δ of the heated inert material is determined by:

$$\delta = \frac{\sqrt{\alpha_i \alpha_r}}{V} \tag{2}$$

where α_i and α_r are the thermal diffusivities of the inert (tile) and reactive materials, respectively, and V is the velocity of the combustion front. Use of this expression in the energy balance leads to a simple relationship between the front velocity V and the combustion temperature T_c:

$$V = \frac{2\alpha_r}{d} \frac{(T_c - T_\infty)}{(T_a - T_c)} \sqrt{\frac{(\lambda\rho c)_i}{(\lambda\rho c)_r}} \tag{3}$$

where T_a is the adiabatic flame temperature, T_∞ is the ambient temperature, T_c is the actual combustion temperature, d is the thickness of the burning layer (i.e., the distance between the two inert media), λ is the thermal conductivity, ρ is the density, and c is the specific heat.

Note that the distance d influences the front velocity V not only as the term in the denominator but also through the combustion temperature T_c: with decreasing the distance, the heat losses increase and the combustion temperature decreases, leading to a lower combustion front velocity and to the appearance of combustion limits. In order to predict the effect of the distance on the front velocity and also determine the quenching distance, it would be convenient to use relationships that do not include the combustion temperature T_c.

For a zero-order reaction and $E/(RT) >> 1$, the combustion front velocity is described by the formula [20], where V_a is the adiabatic combustion front velocity and E is the activation energy:

$$V = V_a \exp\left[-\frac{E(T_a - T_c)}{2RT_aT_c}\right] \tag{4}$$

The reaction rate and hence the adiabatic combustion front velocity are dependent not only on the activation energy, but also on other factors. For example, in experiments [16,23] with cylindrical samples of Al/Ni mixtures, the front velocity ranged from about 10 mm/s to over 100 mm/s, depending on the porosity and particle size of the Al particles. It is also possible that different powders of the same metal may have different impurities and different properties of the oxide layer, which may affect the kinetics unpredictably. Therefore, the adiabatic combustion front

velocity can only be determined experimentally for the mixture of specific powders with specific porosity and particle size.

Using Eqs. 2 and 3, the following transcendental equation has been derived:

$$V \cdot ln\left(\frac{V_a}{V}\right) = \frac{\alpha_r}{d}\frac{E(T_c - T_\infty)}{RT_aT_c}\sqrt{\frac{(\lambda\rho c)_i}{(\lambda\rho c)_r}} \quad (5)$$

Let us assume $T_c = T_a - \Delta T$. The assumption of relatively small heat loss to the inert material allows one to neglect $(\Delta T/T_a)^2$ and $T_\infty \Delta T/ T_a^2$, leading to the following transformation:

$$\frac{T_c - T_\infty}{T_c} = \frac{T_a - \Delta T - T_\infty}{T_a - \Delta T} = \frac{T_a(T_a - T_\infty) - T_\infty \Delta T - \Delta T^2}{T_a^2 - \Delta T^2} = \frac{T_a - T_\infty}{T_a} - \frac{T_\infty \Delta T}{T_a^2} = \frac{T_a - T_\infty}{T_a} \quad (6)$$

Thus, Equation 4 can be replaced with the following equation:

$$V \cdot ln\left(\frac{V_a}{V}\right) = \frac{\alpha_r}{d}\frac{E(T_a - T_\infty)}{RT_a^2}\sqrt{\frac{(\lambda\rho c)_i}{(\lambda\rho c)_r}} \quad (7)$$

It is convenient to use the dimensionless parameter γ [20]:

$$\gamma = \frac{\alpha_r}{V_a d}\frac{E(T_a - T_\infty)}{RT_a^2}\sqrt{\frac{(\lambda\rho c)_i}{(\lambda\rho c)_r}} \quad (8)$$

Then, Equation 6 can be rewritten as:

$$\gamma\left(\frac{V_a}{V}\right) = ln\left(\frac{V_a}{V}\right) \quad (8)$$

The velocity at the quenching distance is less than V_a by e times ($\gamma = e^{-1}$) and the quenching distance for the given V_a can be determined from:

$$d_q = e\frac{\alpha_r}{V_a}\frac{E(T_a - T_\infty)}{RT_a^2}\sqrt{\frac{(\lambda\rho c)_i}{(\lambda\rho c)_r}} \quad (9)$$

Application of Thermophysical Properties to Model

This analysis has been applied to the system under investigation. The activation energy of the Al-Ni reaction was assumed to be 76 kJ/mol [16,23-24]. As noted in the introduction, T_a = 1912 K. The thermophysical properties of the tiles and the reactive mixture were taken as shown in Table 1: a_i = 0.268 mm^2/s, c_i = 1.038 J/(g·K), ρ_i = 1.84 g/cm^3, λ_i = 0.512 W/(m·K), a_r = 0.1 mm^2/s, c_r = 0.719 J/(g·K), ρ_r = 2.10 g/cm^3, λ_r = 0.151 W/(m·K). At these parameters, parameter γ is:

$$\gamma = \frac{0.837 \frac{mm^2}{s}}{V_a d} \tag{10}$$

Solving Equation 8 at γ calculated with Equation 10 for different values of V_a and d generated the dependence of the front velocity on the distance d for each V_a. Also, using Equation 9, the quenching distance was determined for each V_a. To investigate the sensitivity of the theoretical combustion front velocity to thermophysical properties, we have repeated the calculations at the thermal diffusivity of the NiAl product, 7.83 mm^2/s (see Table 3.1), as well as the thermal diffusivity of 1.0 mm^2/s, which is roughly in the middle between the values for the reactive mixture and the combustion product. Figure 4.1 shows the obtained dependencies. For comparison, the experimental front velocities are also shown.

Figure 4.1 shows the obtained dependencies. For each curve, the lowest velocity corresponds to the quenching distance. For comparison, the experimental velocities are shown as well. It is seen that the predicted dependencies qualitatively describe the observed increase in the front velocity with increasing the distance, but there are clear quantitative discrepancies. As compared with the experimental curve, the 0.1 mm^2/s curves have a very small slope in the range of 2-8 mm, while the 7.83 mm^2/s curves predict too large quenching distances. The 1.0 mm^2/s assumption produces a better agreement with the experimental data.

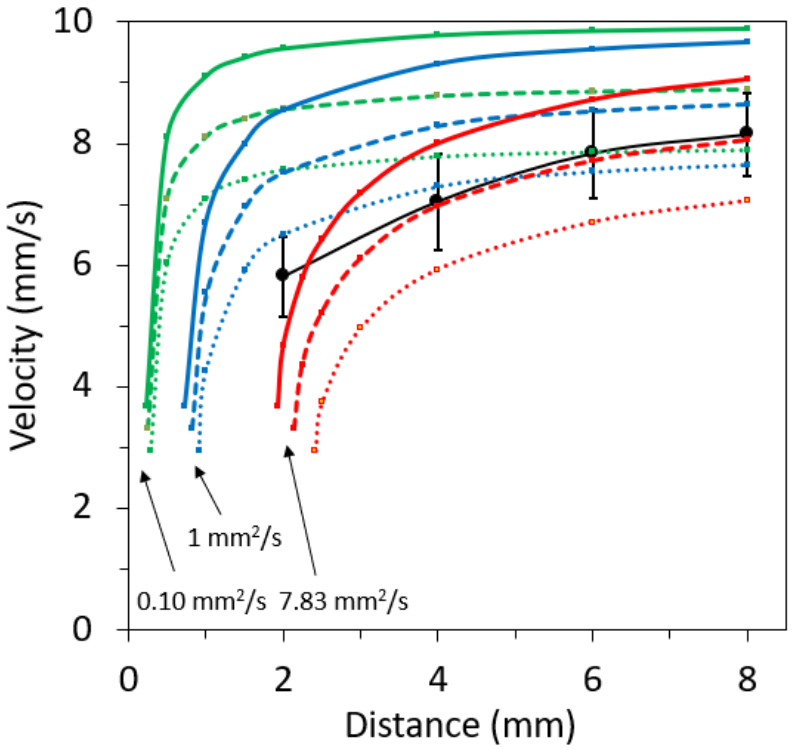

Figure 4.1: The Combustion Front Velocity at Different Values of the Adiabatic Combustion Front Velocity.

Comparison of the experimental and predicted values of the front velocity shows that the adiabatic front velocity may be around 10 mm/s. It might be thought that experiments at larger distances would allow one to determine the adiabatic combustion front velocity, which would prove useful in comparisons of modeling and experimental data. However, it was decided not to conduct experiments at distances larger than 8 mm because the height of the system was only 27.5±0.6 mm and increasing the distance would make the geometric configuration too different from the used two-dimensional setup. Note that increasing the height was technically difficult in the used experimental setup, as the door ports on the vacuum chamber limited the cross-section of what could be placed inside.

The discrepancies between modeling and experimental data could be caused by the assumption of constant thermophysical properties, which were taken at a relatively low temperature in the calculations. In reality, the thermophysical properties of the reactive mixture

are dependent on the temperature and the mixture composition, which are both changing during the process. The observation of a better agreement with experiment at a diffusivity of 1.0 mm^2/s implies that the model works well a that further improvement could be achieved by accounting for the variation of thermophysical properties with temperature.

The discrepancy could also be caused by larger actual heat losses from the reactive mixture than accounted for in the model. The heat losses by radiation are not taken into account in the model, where the system is infinitely long in the vertical direction. This leads to higher temperatures and hence higher velocities in the model. Note that in the applications, radiative heat losses will be less important when thicker tiles are used.

The used assumption of a small heat flux to the tiles as compared with that to the reactive mixture is described by the following inequality [20]:

$$\rho_i c_i \delta \ll \rho_r c_r \frac{d}{2} \tag{12}$$

At d = 2 mm, the heat flux in the right side of Equation 12 is equal to 0.151 J/cm^2-K. Based on Equation 1, the characteristic thickness δ of the heated tile is equal to 0.086 mm at α_r = 1 mm^2/s and V = 6 mm/s. Then the heat flux in the left side of Equation 12 is equal to 0.016 J/cm^2-K, i.e., the assumption is valid. With increasing distance between the tiles, the front velocity increases relatively slowly (see Figures 3.4 and 4.1) and hence the validity of the assumption improves.

An interesting result of both experimental and modeling studies is that the quenching distance in the investigated system is very small, 0.2-0.9 mm in modeling when α_r = 0.1-1 mm^2/s and less than 2 mm in the experiments (it was difficult to conduct experiments at lower distances). This is an encouraging result for space applications because the smaller the distance between the tiles, the smaller amount of metal that is required to be transported from Earth or recovered from in-situ resources.

Chapter 5: Conclusions

Summary of Results

Experiments on the combustion of Al/Ni reactive mixtures between JSC-1A tils under a 1 kPa argon environment have been conducted. Regardless of the experimental gap size, the combustion front consistently propagated between the tiles. This indicates that the real quenching distance is below 2 mm, which is supported by the modeled results. Further, because the combustion front was able to easily propagate in the inert, low pressure atmosphere of the chamber, this suggests that such a combustion joining reaction would likely be able to occur on the Moon or Mars.

Joining of the tiles, however, remained inconsistent in experimental testing. While several experiments resulted in a joint strong enough to support the weight of the tiles, many experiments failed to join the two or four tiles together. In some of these failed trials, however, the NiAl product did join to one of the tiles, but not both. While this is somewhat speculative, this suggests the possibility that thermal contraction pulled the product material off one or both of the tiles during cooling. The pins used to establish the gap prevented the tiles from contracting with the NiAl material.

As expected, front velocity increased with wider experimental gaps. The front velocity seemed to be rising to a limit, the adiabatic velocity, but this exact measure remains unknown, either experimentally or theoretically. The nature of the model assumptions precluded continued widening of the gap, as the height of the tiles in relation to the combustion front could no longer be considered infinite. Temperature measurements proved inconclusive due to an apparent reaction with the thermocouple material.

Testing of the thermophysical properties of the tiles, the reactants, and the products was conducted using differential scanning calorimetry and laser flash analysis. It was found that the NiAl product had a thermal diffusivity and conductivity two orders of magnitude higher than that

of the reactants or tiles, affecting the model assumption that these properties of the reactants and products would be constant.

A two-dimensional model of the steady propagation of the combustion wave over a condensed layer placed between two inert media has been applied to the investigated system. The discrepancy in thermophysical properties led to varying the properties in the system; this led to better agreement between the experimental and modeled results.

Both the modeling and experimental results suggest that the quenching distance in the investigated system is below 2 mm. It was not feasible in the present system to conduct experiments with a smaller experimental gap, and would likely be impractical to attempt in the proposed application. However, the low value does imply that only a small amount of the reactive mixture would be required for joining such tiles on the Moon or Mars.

Future Work

To increase the success of the joining technique, several further areas of interest could be investigated. First, a more exothermic reactive mixture could be examined, such as the titanium-boron system. The increased heat release from the reaction would increase the characteristic thickness of the tiles, and therefore expose a larger volume of the tiles to partial melting. This should increase the interaction zone between the tiles and the reaction product, and improve the qualities of the joining. However, such research would also have to consider the material properties of the joining material, such as brittleness and thermal expansion.

A second area of improvement would involve the experimental setup. Because of the steel pins, the thermal expansion of the product material first pushed against the tiles, and, during cooling, pulled them together. However, because the pins would not allow the tiles to move any closer together, the effect likely became the NiAl product pulling away from the tiles. As a result, the joining failed. This could be improved by using a mechanism to push the two tiles together during combustion, or allow more freedom of movement of the tiles during cooling, perhaps with

some type of spring mechanism. Such a setup should allow the tiles to move with the thermal contraction of the NiAl or other reaction product.

Thirdly, the use of alternating layers of bi-metallic foils may improve the joining properties. Rather than using a relatively low density powder, foils would have the advantage of a higher density reactant.

References

[1] P. H. Cadogan, The Moon- Our Sister Planet, New York, NY: Cambridge University Press, 1981.

[2] G. H. Heiken, D. T. Vaniman and B. M. French, Lunar Sourcebook: A User's Guide to the Moon, New York, NY: Cambridge University Press, 1991.

[3] S. A. Wagner, "The Apollo Experience Lessons LEarned for Constellation Lunar Dust Management," National Aeronautics and Space Administration, Johnson Space Center, Houston, TX, 2006.

[4] C. Immer, P. Metzger, P. E. Hintze, A. Nick and R. Horan, "Apollo 12 Lunar Module exhuast plume impingement on Lunar Surveyor III," *Icarus,* vol. 211, pp. 1089-1102, 2011.

[5] P. T. Metzger, J. E. Lane, C. D. Immer and S. Clements, "Cratering and blowing soil by rocket engines during lunar landings," in *Sixth International Conference on Case Histories in Geotechnical Engineering*, Arlington, 2008.

[6] P. Hintze, "Building a vertical take off and landing pad using in situ materials," in *Space Manufacturing 14: Critical Technologies for Space Settlement- Space Studies Institute*, Mountain View, CA, 2010.

[7] F. Alvarez, C. White and E. Shafirovich, "Combustible mixtures of lunar regolith with metals: Thermodynamic analysis and combbustion experiments," *Journal of Thermophysics and Heat Transfer,* vol. 25, no. 4, pp. 620-625, 2011.

[8] G. Corrias, R. Licheri, R. Orru and G. Cao, "Optimization of the self-propagating high-temperature process for the fabrication in situ of Lunar construction materials," *Chemical Engineering Journal,* Vols. 193-194, pp. 410-421, 2012.

[9] G. Corrias, R. Licheri, R. Orru and G. Cao, "Self-propagating high-temperature synthesis reactions for the fabrication of Lunar and Martian physical assets," *Acta Astonautica,* vol. 70, pp. 69-76, 2012.

[10] A. Delgado and E. Shafirovich, "Towards better combustion of lunar regolith with magnesium," *Combustion and Flame,* vol. 160, pp. 1876-1882, 2013.

[11] A. Delgado, S. Cordova and E. Shafirovich, "Thermite reactions with oxides of iron and silicon during combustion of magnesium with lunar and Martian regolith simulants," *Combustion and Flame,* vol. 162, pp. 3333-3340, 2015.

[12] E. J. Faierson, K. V. Logan, B. K. Stewart and M. K. Hunt, "Demonstration of comcept for fabrication of lunar physical assets utilizing lunar regolith simulant and a geothermite reaction," *Acta Astronautica,* vol. 67, pp. 38-45, 2010.

[13] M. A. Hobosyan and K. S. Martirosyan, "Consolidation of lunar regolith simulant by activated thermite reactions," *Journal of Aerospace Engineering,* vol. 28, no. 4, pp. 04014105-1-9, 2015.

[14] C.S. Ray, S.T. Reis, S. Sen, and J.S. O'Dell, "JSC-1A lunar soil simulant: Characterization, glass formation, and selected glass properties," *Journal of Non-Crystalline Solids*, vol. 356, pp. 2369-2374, 2010.

[15] K. Morsi, "The diversity of combustion synthesis processing: a review," *Journal of Material Science,* vol. 47, pp. 68-92, 2012.

[16] Y. S. Naiborodenko and V. S. Itin, "Gasless combustion of metal powder mixtures 1. Mechanism and details," *Fizika Goreniya i Vzryva,* vol. 11, no. 3, pp. 343-353, 1975.

[17] E. A. Levashov, A. S. Mukasyan, A. S. Rogachev and D. V. Shtansky, "Self-propagating high-temperature synthesis of advanced materials and coatings," *International Materials Review,* vol. 62, no. 4, pp. 203-239, 2017.

[18] J. J. Moore and H. J. Feng, "Combustion synthesis of advanced materials: Part I. Reaction Parameters," *Progress in Materials Science,* vol. 39, pp. 243-273, 1995.

[19] M.W. Chase, Jr., NIST-JANAF Thermochemical Tables, Fourth Edition, J. Phys. Chem. Ref. Data, Monograph 9 (1998) 1-1951.

[20] H. Zhang, P. Feng, F. Akhtar, "Aluminium matrix tungsten aluminide and tungsten reinforced composites by solid-state diffusion mechanism," *Scientific Reports*, 7 (2017) 12391.

[21] S.S. Rybanin and S.L. Sobolev, "Velocity and combustion limits in a thermally thin condensed substance layer undergoing heat exchange with an inert medium," *Fizika Goreniya i Vzryva,* 25 (5) (1989) 524-531.

[22] S.S. Rybanin and S.L. Sobolev, "Velocity and combustion limits in a thermally thick condensed substance layer undergoing heat exchange with an inert medium," *Fizika Goreniya i Vzryva,* 25 (5) (1989) 531-540.

[23] Yu.S. Naiborodenko, V.I. Itin, “Gasless combustion of metal powders. II. Effect of mixture composition on the combustion rate and the phase composition of the products,” *Fizika Goreniya i Vzryva* 11 (5) (1975) 626-629.

[24] S. Gennari, F. Maglia, U. Anselmi-Tamburini, G. Spinolo, “Self-propagating high-temperature synthesis of intermetallic compounds: a computer simulation approach to the chemical mechanisms,” *Journal of Physical Chemistry,* B 107 (2003) 732-738.

Vita

Robert E. Ferguson II was born in Tampa, FL, graduating from Bloomingdale High School. He served in the United States Army from 2000-2013, and was awarded a Bronze Star for service in Afghanistan. After leaving the Army he enrolled at the University of Texas at El Paso. In the spring of 2016, he began working with Dr. Evgeny Shafirovich and the Center for Space Exploration and Technology Research at UTEP, focusing on thermal decomposition of green monopropellants. He graduated Magna Cum Laude with his Bachelor's of Science in Mechanical Engineering in Spring 2016. Staying at UTEP to continue working on a master's degree, he was awarded the NASA Harriet G. Jenkins Graduate Fellowship to pursue work in combustion joining of regolith tiles. He has presented his work at the Southwest Emerging Technology Symposium (2016, 2017, 2018), the Space Resource Roundtable (2017), the Low Cost Planetary Missions Conference (2017), the Materials Research Society Fall Meeting (2017), and the American Society of Civil Engineers Earth and Space Conference (2018).

Permanent address: 300 El Puente Drive
El Paso, TX 79912

This thesis was typed by Robert E. Ferguson II.